

# NURBS-ENHANCED FINITE ELEMENT METHOD

R. Sevilla\*, S. Fernández-Méndez\* and A. Huerta\*

\*Laboratori de Càlcul Numèric (LaCàN)  
Departament de Matemàtica Aplicada III  
Universitat Politècnica de Catalunya  
e-mail: {ruben.sevilla,sonia.fernandez,antonio.huerta}@upc.edu  
web page: <http://www-lacan.upc.edu>

**Key words:** NURBS, Finite Elements, CAD, exact geometry representation, high-order isoparametric finite elements, Discontinuous Galerkin

**Abstract.** *An improvement of the classical finite element method is proposed. It considers an exact representation of the geometry by means of the usual CAD description of the boundary with Non-Uniform Rational B-Splines (NURBS). For elements not intersecting the boundary, a standard finite element interpolation and numerical integration is used. Specifically designed piecewise polynomial interpolation and numerical integration are proposed for those finite elements intersecting the NURBS boundary. Numerical examples with a Discontinuous Galerkin formulation are shown in order to demonstrate the applicability and behavior of the proposed methodology. The results are encouraging and show that NEFEM is more accurate than the corresponding isoparametric finite elements.*

## 1 INTRODUCTION

The relevance of an accurate representation of the domain and its boundary has recently been pointed out by several authors, see<sup>1,2,3,4,5</sup> among others. In some applications, such as compressible flow problems, an important loss of accuracy is observed when a linear approximation of the boundary is used, see<sup>1,2</sup>. Reference<sup>1</sup> shows that, in the presence of curved boundaries, a meaningful high-order accurate solution can be obtained only if a corresponding high-order approximation of the geometry is employed (i.e. isoparametric finite elements). A detailed analysis of this problem is performed in<sup>5</sup>. In this work, it is shown that for a consistent boundary discretization in a discontinuous Galerkin finite element method it is necessary to take into account the effect of the domain boundary curvature. However, the need of an accurate representation of the geometry is not an exclusive matter of fluid mechanics. For instance, similar conclusions are derived in<sup>3</sup> for linear elasticity problems: sizable errors are present in the numerical solution when the order for the geometric approximation is lower than the order of functional interpolation, even for geometries as simple as a sphere. Isoparametric finite elements or superparametric finite elements (i.e. greater order for the geometry) are necessary in order to ensure

an accurate enough representation of the geometry. On the other hand, reference<sup>4</sup> analyzes the error induced by the approximation of curvilinear geometries with isoparametric elements. The 3D Maxwell equations are solved in a sphere with isoparametric finite elements and with an exact mapping of the geometry. The exact mapping provides more accurate results, with errors differing by an order of magnitude. Thus, in some applications, an isoparametric representation of the geometry is far from providing an optimal numerical solution for a given finite element discretization.

Recently,<sup>6</sup> proposes a new methodology: the *isogeometric analysis*. Its goal is to consider an exact representation of the geometry, with no dependency on the spatial discretization. In the *isogeometric analysis* the solution of the boundary value problem is approximated with the same NURBS (*Non-Uniform Rational B-Splines*,<sup>7</sup>) base used for the description of the geometry.

The methodology proposed in this paper follows the same rationale but is more simple because NURBS are restricted to the boundary of the computational domain, which is the one that usually is directly related to a CAD. Thus, *NURBS-Enhanced Finite Element Method* (NEFEM) considers the exact NURBS description for the computational domain and the solution is approximated with standard finite element (FE) polynomial interpolation. Moreover, in the large majority of the domain (i.e., in the interior) —for elements not intersecting the boundary— a standard FE interpolation and numerical integration is used, preserving the computational efficiency of classical finite element techniques. Specifically designed piecewise polynomial interpolation and numerical integration is proposed for those finite elements along the NURBS boundary.

The use of a piecewise polynomial approximation represents an important advantage in front of the NURBS functional approximation used in the *isogeometric analysis*: the NEFEM ensures the local reproducibility of polynomials and, therefore, it preserves the classical FE convergence properties.

Section 2 presents the basic concepts and fundamentals of the NEFEM. Special attention is paid to the interpolation and numerical integration in those elements affected by the NURBS description of the boundary. In order to facilitate the explanation, the NEFEM is presented for 2D domains. Although more attention is required to geometrical aspects, the generalization to 3D domains is straightforward. In section 3, a numerical example demonstrate the competitiveness of the NEFEM in front of isoparametric finite elements for the solution of transient electromagnetic scattering problems. Finally, in section 4 the conclusions of this work are presented.

## 2 NURBS-ENHANCED FINITE ELEMENT METHOD (NEFEM)

A domain  $\Omega \subset \mathbb{R}^2$  is considered, whose boundary  $\partial\Omega$ , or a portion of its boundary, is defined by NURBS curves<sup>7</sup>. Every NURBS is assumed to be parameterized by

$$\mathbf{N} : [0, 1] \longrightarrow \mathbf{N}([0, 1]) \subseteq \partial\Omega \subset \mathbb{R}^2. \quad (1)$$

A triangularization of the domain  $\bar{\Omega} = \bigcup_e \bar{\Omega}_e$  is also assumed, such that every triangle  $\Omega_e$  has at most one side on the NURBS boundary. Figure 1 shows a domain with part of the boundary described by a NURBS circular curve and a valid triangulation for the NEFEM.



Figure 1: Physical domain with part of the boundary defined by a circular NURBS curve (left) and a valid triangulation for the NEFEM (right)

At all elements whose boundary does not intersect the NURBS boundary, the usual FE interpolation and numerical integration is considered. Thus, this section is devoted to the definition of the interpolation and the numerical integration at an element with one side on the NURBS boundary. Say, an element  $\Omega_e$  with two straight interior sides and one side defined by a trimmed NURBS,

$$\Gamma_e = \mathbf{N}([u_1^e, u_2^e]),$$

with  $0 \leq u_1^e < u_2^e \leq 1$ . There are no restrictions in the location of the nodes in the NURBS boundary. The NURBS parametrization can change its definition inside one edge. That is, it is possible to have a *breakpoint*<sup>7</sup> on  $(u_1^e, u_2^e)$ . This is another advantage with respect to the isogeometric analysis<sup>6</sup>.

For each element  $\Omega_e$ , a triangle  $T_e$  is defined using its vertices, see figure 2. Then, a



Figure 2: Physic element  $\Omega_e$  (left) and triangle  $T_e$  defined using its vertices (right)

linear transformation  $\Psi : I \longrightarrow T_e$  is used. It goes from the reference triangle  $I$  to the triangle  $T_e$ , see Figure 3.

**Remark 1** *In order to simplify the presentation, it is assumed that the interior vertex of  $T_e$  is mapped to the vertex  $(-1, 1)$  in  $I$ . The implementation of this condition only requires a proper local numbering of the vertices of the element.*

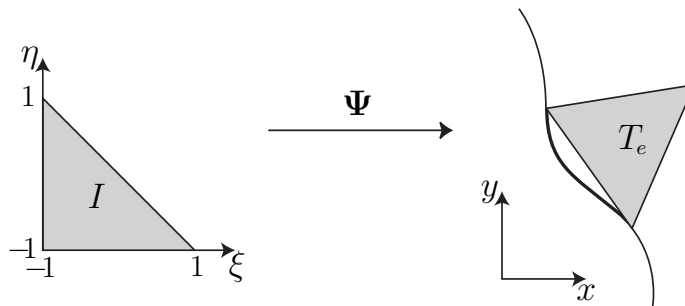


Figure 3: Mapping  $\Psi$  defined as a linear transformation from the reference triangle  $I$  to the triangle  $T_e$  (given by the vertices of  $\Omega_e$ )

Note that the inverse of this linear transformation maps the triangle  $T_e$  into the reference triangle  $I$ , but also maps the physic element  $\Omega_e$  into a curved element in local coordinates with two straight sides, namely

$$I_e := \Psi^{-1}(\Omega_e), \quad (2)$$

see Figure 4.  $I_e$  is called the *local curved element* for the physic element  $\Omega_e$ .

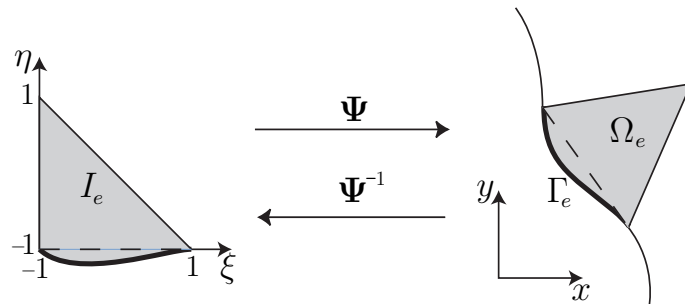


Figure 4: Linear transformation mapping the local curved element  $I_e$  to the physic element  $\Omega_e$

Note that the reference triangle  $I$  is the same for all elements  $\Omega_e$ . However, the local curved element  $I_e$  depends on the trimmed NURBS defining the curved side  $\Gamma_e$  of  $\Omega_e$ , and therefore it is different for every element  $\Omega_e$  intersecting the NURBS boundary.

**Remark 2** *The use of a linear transformation from the local coordinates  $\xi$  in  $I_e$  to the cartesian coordinates  $x$  in  $\Omega_e$ , ensures that a polynomial interpolation of degree  $m$  in  $\xi$  leads to a polynomial interpolation with the same degree in  $x$ . Thus, the consistency and accuracy of the approximation is ensured even for elements  $\Omega_e$  far from being a straight-sided element.*

Under these assumptions, the FE interpolation base and the numerical integration to be used are proposed next.

## 2.1 FE polynomial base

The usual nodal interpolation defined by the Lagrange polynomials is considered in  $I_e$ , or equivalently, in  $\Omega_e$ . The implementation proposed in<sup>8</sup> is adopted, in order to compute the Lagrange polynomials,  $\{L_i(\boldsymbol{\xi})\}_{i=1}^{n_{nodes}}$ , for any order and for any distribution of nodes. An orthogonal polynomial base  $\{p_i\}_{i=1}^{n_{nodes}}$  is considered in  $I_e$ , with no dependency on the nodal coordinates  $\{\boldsymbol{\xi}_i\}_{i=1}^{n_{nodes}}$ . The Lagrange polynomial base is then obtained as

$$L_i = \sum_{j=1}^{n_{nodes}} [\mathbf{V}^{-1}]_{ji} p_j, \quad (3)$$

with the Vandermonde matrix  $V_{ij} := p_j(\boldsymbol{\xi}_i)$ , for  $i, j = 1, \dots, n_{nodes}$ .

**Remark 3** *Note that any polynomial base  $\{p_i\}$ , with no dependency on the nodal coordinates, can be considered for the computation of the Lagrange polynomials using (3). However, an orthogonal polynomial base  $\{p_i\}_{i=1}^{n_{nodes}}$ , such as the one derived from Jacoby polynomials<sup>8,9,10,11</sup>, is advisable in order to ensure a moderate condition number for the Vandermonde matrix  $\mathbf{V}$ . This base also allows an analytical computation of some inner products.*

From an implementation point of view, it is worth noting that all elemental matrices can be first computed for the orthogonal polynomial base, and then transformed with the Vandermonde matrix. That is, let  $\mathbf{M}_e^p$  be an elemental matrix computed in terms of the orthogonal polynomial base, then  $\mathbf{M}_e = \mathbf{V}^{-T} \mathbf{M}_e^p \mathbf{V}^{-1}$  is the corresponding elemental matrix for the Lagrange nodal base.

This paper considers equally-spaced distributions of nodes in  $I_e$ , see left distribution in Figure 5. It corresponds to the usual nodal distribution for the reference triangle  $I$ . Other nodal distributions can also be used. For instance, the right distribution in Figure 5 is adapted in order to locate nodes along the NURBS side. This option makes sense if one wants to set nodal values along the boundary, but it does not represent any advantage if boundary conditions are imposed in weak form, as usual in Discontinuous Galerkin formulations. Moreover, in this case nodal coordinates depend on the local curved triangle  $I_e$  reducing the computational efficiency of the approach, and leading to a different Vandermonde matrix for each curved element. The use of a nodal distribution with no dependency on the local curved element  $I_e$ , such as the left distribution, is more efficient because of the unique definition of the nodal coordinates and the unique computation of the Vandermonde matrix, with no dependency of the curved element.

Although equally-spaced nodal distributions are assumed in the rest of the paper, it is worth noting that for high-order interpolation ( $\geq 5$ -th order) it can be more convenient to use special distributions of nodes in order to reduce the condition number of the resulting elemental matrices, see<sup>12</sup> for details. Moreover, numerical experiments reveals that, using a distribution of nodes adapted to the NURBS side, the condition number of the elemental matrices is reduced two or three times, in comparison with the same distribution of nodes located in the reference triangle  $I$ .

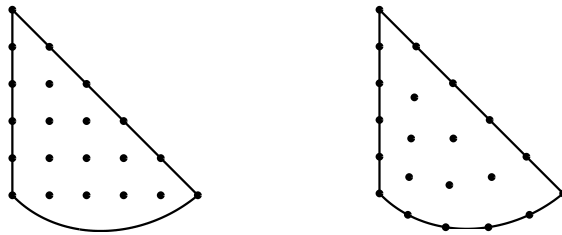


Figure 5: 5th-order nodal distributions in  $I_e$ : for equally-spaced nodes (left) and adapted to the NURBS side (right)

## 2.2 Numerical integration

NEFEM requires computing integrals of functions  $f$  along an edge given by a trimmed NURBS  $\Gamma_e = \mathbf{N}([u_1^e, u_2^e])$ , that is

$$\int_{\Gamma_e} f \, dl = \int_{u_1^e}^{u_2^e} f(\mathbf{N}(u)) |J_{\mathbf{N}}(u)| \, du, \quad (4)$$

where  $|J_{\mathbf{N}}|$  denotes the Jacobian of the NURBS parametrization  $\mathbf{N}$ . As usual, a 1D numerical quadrature is used for the numerical computation of the integral.

It is important to note that the parametrization of a trimmed NURBS,  $\mathbf{N}$ , is a piecewise rational function whose definition changes at the so called *breakpoints*<sup>7</sup>. Thus, an independent numerical quadrature must be considered for each one of the intervals between breakpoints in order to take into account the discontinuous nature of the parametrization. Numerical experiments reveal that Gauss-Legendre quadratures are a competitive choice in front of other quadrature rules.

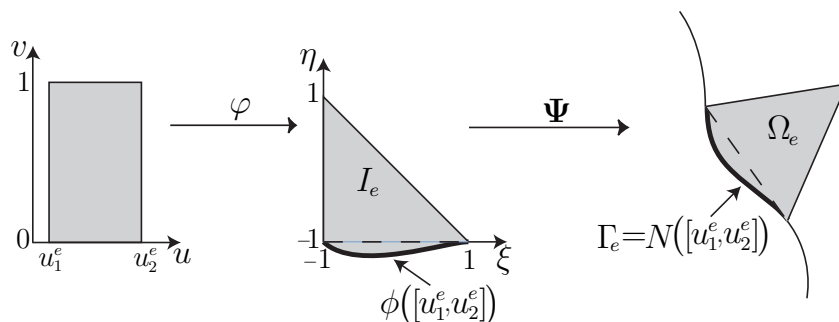
NEFEM also requires computing integrals over an element  $\Omega_e$  with one side  $\Gamma_e$  on the NURBS boundary (see Figure 4), that is

$$\int_{\Omega_e} f \, dx \, dy = |J_{\Psi}| \int_{I_e} f \, d\xi \, d\eta \quad (5)$$

where  $|J_{\Psi}|$  is the Jacobian of the linear transformation  $\Psi$ . The computation of (5) requires a numerical quadrature for every curved element  $I_e$ . The proposed strategy corresponds to the definition of a transformation from the rectangle  $[u_1^e, u_2^e] \times [0, 1]$  to the curved element  $I_e$ , see Figure 6. That is,  $\varphi = (\varphi_1, \varphi_2) : [u_1^e, u_2^e] \times [0, 1] \rightarrow I_e$  given by

$$\varphi_1(u, v) := 2(1 - v)\phi_1(u) - 1, \quad \varphi_2(u, v) := 2(1 - v)\phi_2(u) + 2v - 1$$

where  $\phi = (\phi_1, \phi_2) := \Psi^{-1} \circ \mathbf{N}$  is the parametrization of the trimmed NURBS corresponding to the curved side in  $I_e$ . Note that this transformation is only valid under the assumption in Remark 1.


 Figure 6: Transformation from  $[u_1^e, u_2^e] \times [0, 1]$  to  $I_e$  and  $\Omega_e$ 

The use of a transformation from the reference triangle  $I$  into the local curved triangle  $I_e$ , in order to use quadratures specifically designed for triangles<sup>13,14</sup> is also studied. For standard finite elements these triangle quadratures require less integration points than other quadratures to achieve the same order and accuracy, but this is not the case for NEFEM elements with a curved side. The use of a transformation depending on the NURBS parametrization  $\phi$  leads to too expensive triangle quadratures. The integration strategy proposed in this section is much more competitive. For example, Figure 7 shows the integration points, for the computation of the integral  $\int_{\Omega_e} x^{10} d\Omega$  with an error of about 0.5%, using the transformation depicted in Figure 6 (left, with 30 integration points) and using a classical triangle quadrature (right, with 54 integration points).

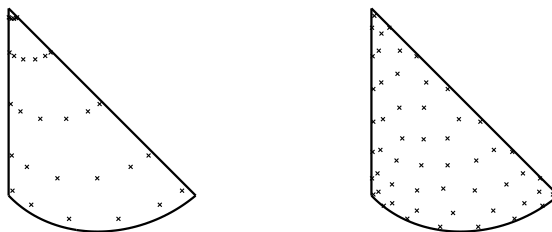


Figure 7: Two numerical quadratures in a curved element

### 3 NUMERICAL EXAMPLE

The transient Maxwell's equations are considered for the simulation of 2D scattering of a single plane incident electromagnetic wave by an obstacle, assumed to be surrounded by free space.

The *Transverse Electric* (TE) 2D Maxwell equations, in free space, for a linear isotropic material of relative permittivity  $\varepsilon$  and relative permeability  $\mu$ , can be written in dimen-

sionless conservative form as

$$\frac{\partial \mathbf{U}}{\partial t} + \frac{\partial \mathbf{F}_k(\mathbf{U})}{\partial x_k} = \mathbf{0} \quad \text{in } \Omega, \quad (6)$$

where  $\mathbf{U}$  is the vector of conserved quantities

$$\mathbf{U} = (\varepsilon E_1, \varepsilon E_2, \mu H_3)^T, \quad (7)$$

$\mathbf{F}_1$  and  $\mathbf{F}_2$  are the fluxes

$$\mathbf{F}_1 = (0, H_3, E_2)^T \quad \mathbf{F}_2 = (-H_3, 0, -E_1)^T, \quad (8)$$

and  $\mathbf{E} = (E_1, E_2, 0)^T$  and  $\mathbf{H} = (0, 0, H_3)^T$  denote the *scattered* electric and magnetic field intensity vectors. It is assumed that there are no electric sources in the material.

Figure 8 shows the computational mesh used for the simulations. The obstacle consists on a perfectly conducting circular cylinder defined by a NURBS curve, and the incoming plane wave travels in the  $x^+$  direction with a unitary velocity. The exact geometry is represented using one quadratic NURBS and only four elements are considered in the NURBS boundary.

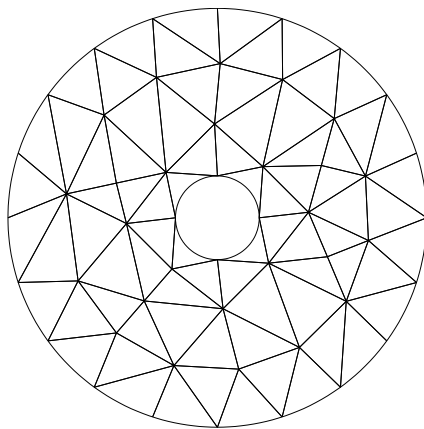


Figure 8: Computational mesh

The time marching is performed using a fourth-order explicit Runge-Kutta scheme. Figure 9 shows the numerical solution obtained after four cycles.

The Radar Cross Section (RCS) is represented in figure 10. The RCS distribution is in excellent agreement with the analytical one. The RCS is a quantity of interest in electromagnetic scattering problems and it is defined as

$$RCS = 10 \log_{10}(\sigma), \quad (9)$$

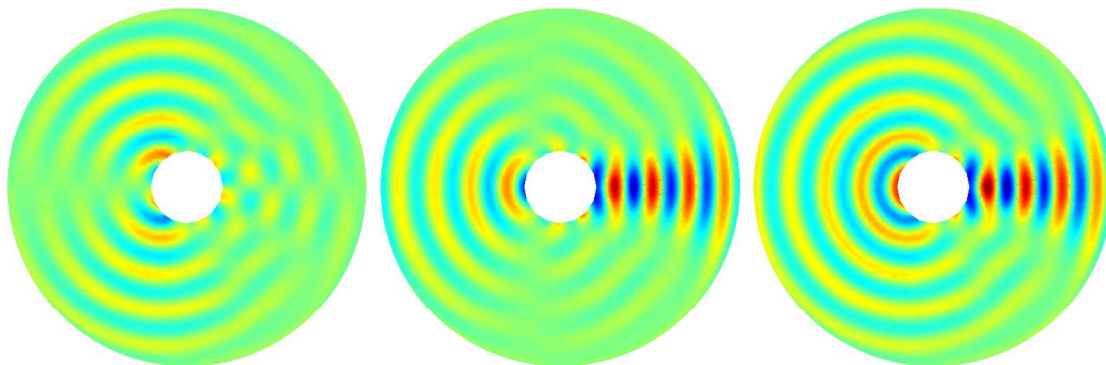


Figure 9: Solution,  $E_1$  (left),  $E_2$  (center) and  $H_3$  (right), after four cycles using the NEFEM with a 9th degree of interpolation

where  $\sigma$  is the scattering width, see<sup>15</sup>. Considering the TE mode for a two dimensional target, it is defined as

$$\sigma(\phi) = \lim_{r \rightarrow \infty} 2\pi r \frac{|\tilde{H}_3|^2}{|\tilde{H}_3^I|^2} \quad (10)$$

where  $(r, \phi)$  are the cylindrical polar coordinates and the tilde indicates that the time-harmonic component of this field is removed, that is  $\tilde{H}_3 := H_3 e^{-jkt}$  where  $j = \sqrt{-1}$  and  $k$  is the dimensionless wavenumber. Using a near to far-field transformation<sup>16</sup>, the scattering width is computed as

$$\sigma = \frac{k}{4} \int_C [n_2 \tilde{H}_3 \sin(\phi) + n_1 \tilde{H}_3 \cos(\phi) + \sqrt{\frac{\mu}{\epsilon}} \tilde{\alpha}] e^{jk[x'_1 \cos(\phi) + x'_2 \sin(\phi)]} dx'_1 dx'_2 \quad (11)$$

where  $C$  is a closed curve surrounding the obstacle and  $\tilde{\alpha} := \alpha e^{-jkt}$ .

The absolute value of the error in the RCS is represented in figure 11 for isoparametric finite elements and for the NEFEM using a degree of interpolation  $p = 6 \dots 9$ . The results using a degree of interpolation  $p = 1 \dots 5$  are not of interest. For example, with  $p = 5$  only 6 degrees of freedom on each wave length are considered.

As expected, the maximum error is always concentrated in the zones with sharp variations in the RCS. Moreover, it can be observed in figure 11 that the RCS distribution is asymmetric. It is caused by the asymmetry of the computational mesh, not by the boundary description. Increasing the order of the polynomials the RCS error is always reduced, except for the computation with  $p = 8$  and  $p = 9$ . This loss of precision is observed using isoparametric finite elements and the NEFEM.

In all the cases, the error using classical isoparametric elements is higher than using the NEFEM, see 1. More precisely, the results summarized in this table show that, for a given degree of interpolation, the NEFEM is between 11 and 15 times more accurate than isoparametric finite elements.

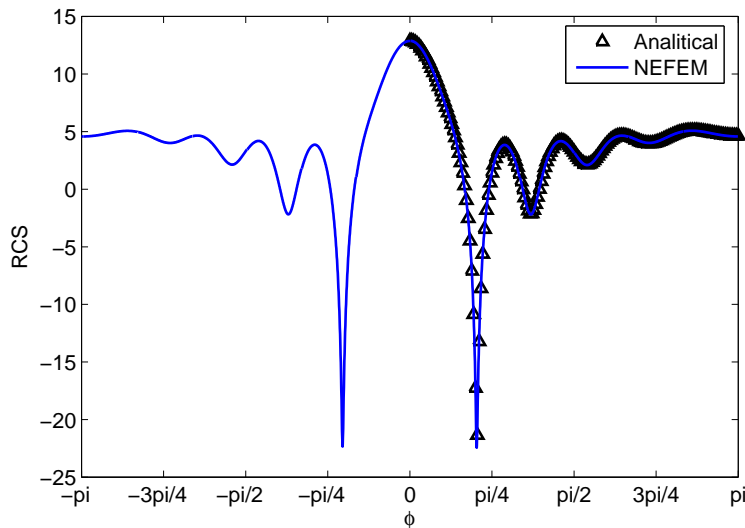


Figure 10: RCS for the example of figure 9

p	DG	DG-NEFEM	Ratio
6	0.3751	0.0338	11.1
7	0.3044	0.0200	15.2
8	0.1163	0.0091	12.8
9	0.2059	0.0174	11.8

Table 1: RCS error in the maximum norm with isoparametric finite elements and the DG-NEFEM, and ratio between the DG error and the DG-NEFEM error

#### 4 CONCLUDING REMARKS

In this paper an improvement of the classical finite element method has been proposed for a standard continuous formulation and also for a Discontinuous Galerkin formulation. It considers the exact geometric model by means of the CAD description of the boundary of the domain using Non-Uniform Rational B-Splines. Then, for elements intersecting the boundary a specifically designed polynomial interpolation and numerical integration is proposed.

Numerical examples involving electromagnetic scattering show the advantages of the NEFEM, in front of standard isoparametric finite elements, when it is important to work with an accurate geometric model and to ensure a high precision of the functional approximation on the boundary. The performed analysis is encouraging and the numerical examples reveal that the NEFEM is at least 11 times more accurate than the standard isoparametric finite elements for a given degree of interpolation.

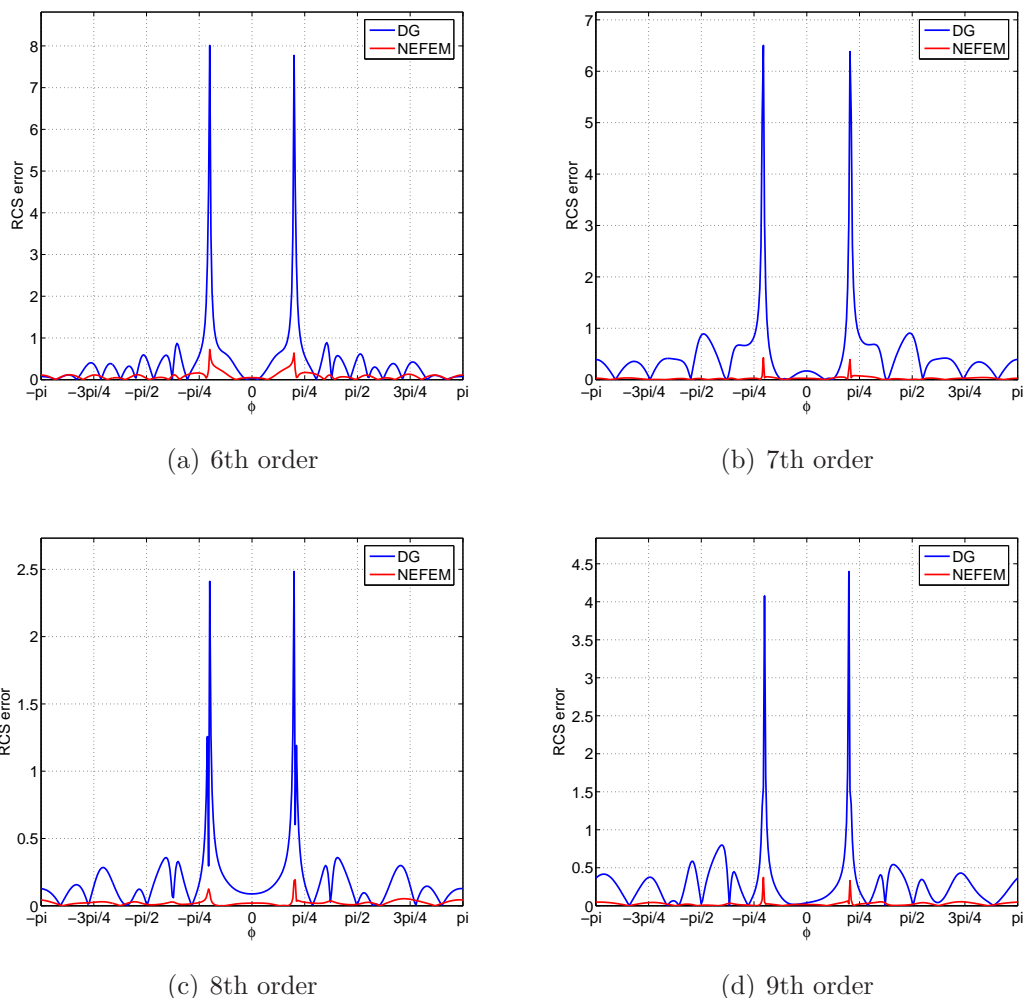


Figure 11: Absolute value of the RCS error with a degree of interpolation  $p = 6 \dots 9$

## ACKNOWLEDGEMENTS

The authors are partially supported by the *Ministerio de Educación y Ciencia* (grant number DPI2004-03000). The authors also would express his gratitude to the *Departament de Matemàtica Aplicada III* and the *Escola d'Enginyers Camins Canals i Ports de Barcelona* for the partial support of this work.

## References

- [1] F. Bassi, S. Rebay, High-order accurate discontinuous finite element solution of the 2D Euler equations, *J. Comput. Phys.* 138 (2) (1997) 251–285.
- [2] T. Barth, Simplified numerical methods for gas dynamics systems on triangulated

- domains, Ph.D. thesis, Department of Aeronautics and Astronautics, Stanford University (1998).
- [3] M. X.J.Luo, J.F.Remacle, Influence of geometric approximation on the accuracy of higher order methods, SCOREC report 1.
- [4] D. Xue, L. Demkowicz, Control of geometry induced error in hp finite element (FE) simulations. I. Evaluation of FE error for curvilinear geometries, *Int. J. Numer. Anal. Model.* 2 (2005) 283–300.
- [5] J. Van der Vegt, H. Van der Ven, Discontinuous galerkin discretizations of the euler equations of gas dynamics, in: H. A. Mang, F. G. Rammerstorfer, J. Eberhardsteiner (Eds.), *Proceedings of the Fifth World Congress on Computational Mechanics (WCCM V)*, Vienna University of Technology, 2002.
- [6] T.J.R. Hughes, J.A. Cottrell, Y. Bazilevs, Isogeometric analysis: CAD, finite elements, NURBS, exact geometry and mesh refinement, *Comput. Methods Appl. Mech. Eng.* 194 (39–41) (2005) 4135–4195.
- [7] L. Piegl, W. Tiller, *The NURBS Book*, Springer-Verlag, London, 1995.
- [8] J. S. Hesthaven, T. Warburton, Nodal high-order methods on unstructured grids. I. Time-domain solution of maxwell’s equations, *J. Comput. Phys.* 181 (1) (2002) 186–221.
- [9] G. E. Karniadakis, S. J. Sherwin, *Spectral/hp Element methods for CFD*, Numerical Mathematics and Scientific computation, Oxford University Press, 1999.
- [10] G. Szegő, *Orthogonal Polynomials* (fourth edition), American Mathematical Society, Providence, 1975.
- [11] M. Dubiner, Spectral methods on triangles and other domains, *J. Sci. Comput.* 6 (1991) 345–390.
- [12] Q. Chen, I. Babuška, Approximate optimal points for polynomial interpolation of real functions in an interval and in a triangle, *Comput. Methods Appl. Mech. Eng.* 128 (3–4) (1995) 405–417.
- [13] R. Cools, An encyclopaedia of cubature formulas, *J. Complexity* 19 (3) (2003) 445–453.
- [14] S. Wandzura, H. Xiao, Symmetric quadrature rules on a triangle, *Comput. Math. Appl.* 45 (12) (2003) 1829–1840.
- [15] C. A. Balanis, *Advanced engineering electromagnetics*, J. W. and Sons, New York, 1989.

- [16] A. Taflove, Computational Electrodynamics: The Finite-Difference Time-Domain Method, Artech House, Inc., 1995.